ChemPubSoc Europe

DOI: 10.1002/chem.201804771

CHEMISTRY A European Journal Full Paper

DNA structures | *Hot Paper*

Towards the Development of Photo-Reactive Ruthenium(II) Complexes Targeting Telomeric G-Quadruplex DNA

Justin Weynand,[a, b] Aurélie Diman,[c] Michaël Abraham,[a] Lionel Marcélis,[a] Hélène Jamet,[b] Anabelle Decottignies,[c] Jérôme Dejeu,[b] Eric Defrancq,*[b] and Benjamin Elias*[a]

Abstract: The design and characterization of new ruthenium(II) complexes aimed at targeting G-quadruplex DNA is reported. Importantly, these complexes are based on oxidizing 1,4,5,8-tetraazaphenanthrene (TAP) ancillary ligands known to favour photo-induced electron transfer (PET) with DNA. The photochemistry of complexes **1**–**4** has been studied by classical methods, which revealed two of them to be capable of photo-abstracting an electron from guanine. From studies of the interactions with DNA through luminescence, circular dichroism, bio-layer interferometry, and surface plasmon resonance experiments, we have demonstrated the selectivity of these complexes for telomeric G-quadruplex DNA over duplex DNA. Preliminary biological studies of these complexes have been performed: two of them showed remarkable photo-cytotoxicity towards telomerase-negative U2OS osteosarcoma cells, whereas very low mortality was observed in the dark at the same photo-drug concentration.

Introduction

DNA is considered as an interesting target for developing novel classes of therapeutic agents. Until recently, the focus has been on double-stranded DNA structures (duplex DNA), in which two sequences of DNA are held together in an antiparallel double-helical architecture through canonical Watson–Crick A/T and G/C base pairing. Duplex DNA has mainly been targeted by using intercalators (i.e., small molecules that interact with DNA through intercalation between two adjacent base pairs) or groove binders (i.e., small molecules that interact with DNA in the minor and/or major groove regions).[1] More recently, targeting alternative DNA architectures, in particular G-quadruplexes (G4s), has been increasingly pursued. G-quadruplexes are secondary DNA structures found in guanine-rich sequences. The basic unit is called a G-quartet, which corresponds to the coplanar arrangement of four guanine bases held together by Hoogsteen hydrogen bonds and stabilized by physiologically abundant Na^+ or K^+ cations. G-quartets can stack to form G-quadruplexes, which can adopt a wide variety of topologies according to the number of strands involved in the structure, the strand direction, and variations in loop size and sequence.[2–4] Sequencing and bioinformatics analyses of the human genome indicate that it contains as many as 700 000 sequences of potential G-quadruplex structures (PQS). Interestingly, these putative G-quadruplex-forming sequences are not distributed randomly in the genome. Indeed, a statistically significant enrichment of PQS has been found in several relevant domains of the human genome, including the telomeric region and promoter regions of a number of genes, such as the proto-oncogenes c-Myc, c-Kit, bcl-2, and KRAS, as well as in viruses.[5,6] Strong arguments have recently been presented in favour of the formation of G-quadruplex DNA structures within cells by using G-quadruplex antibodies as well as binding-activated fluorescent G4-targeting ligands.[7–9] Several G4-binding regulatory proteins have been identified, and G4 formation is now suspected to be involved in numerous pathogenic processes, including degenerative disorders, oncogene regulation, and viral infections. Taken together, these data consistently point to a biologically relevant regulatory role for G-quadruplexes.

In this context, the biological functions of G4s are certainly the most documented for the telomeric region. Human telomeric DNA is made of a repeat of the sequence $^{5'}$TTAGGG$^{3'}$ and it is widely accepted that telomeric DNA plays important roles in the development of cancer cells.[10,11] In healthy cells, the telomere shortens after each cell division, and when a limit is reached (i.e., the Hayflick limit), the cell enters into senescence. In most cancer cells, however, the telomere length is main-

[a] J. Weynand, M. Abraham, Dr. L. Marcélis, Prof. Dr. B. Elias
Université catholique de Louvain (UCLouvain)
Institut de la Matière Condensée et des Nanosciences (IMCN), Molecular Chemistry, Materials and Catalysis (MOST)
Place Louis Pasteur 1, bte L4.01.02, 1348 Louvain-la-Neuve (Belgium)
E-mail: Benjamin.Elias@uclouvain.be

[b] J. Weynand, Dr. H. Jamet, Dr. J. Dejeu, Prof. Dr. E. Defrancq
Université Grenoble-Alpes (UGA)
Département de Chimie Moléculaire, UMR CNRS 5250, CS 40700
38058 Grenoble (France)
E-mail: Eric.Defrancq@univ-grenoble-alpes.fr

[c] Dr. A. Diman, Prof. Dr. A. Decottignies
Université catholique de Louvain (UCLouvain) de Duve Institute
Avenue Hippocrate 75 1200 Brussels (Belgium)

Supporting information and the ORCID identification numbers for the authors of this article can be found under:
https://doi.org/10.1002/chem.201804771: Copies of NMR and mass spectra, absorption and luminescence spectra, cyclic voltammograms, CD, BLI, and SPR sensorgrams and microscope images of cells.

tained, leading to replicative immortality. Two different processes are involved in telomere maintenance: (i) overexpression of the telomerase enzyme, which adds copies of telomeric repeats at the chromosome ends,[12] and (ii) the homologous recombination-based mechanism, termed alternative lengthening of telomeres (ALT).[13,14] Telomerase overexpression is observed in almost 85% of cancers, whereas the ALT mechanism is active in 5–10% of cases (in particular in osteosarcoma and glioblastoma).

Over the past decade, a number of small molecules (termed G-quadruplex ligands), displaying varying degrees of affinity and more importantly selectivity (i.e., an ability to interact only with quadruplex DNA and not with duplex DNA), have been designed to target G-quadruplex DNA.[15–19] Most of these molecules have been built from an aromatic core, capable of interacting with G-quadruplex motifs through π-stacking, and decorated with substituents (often positively charged) that can interact with G-quadruplex grooves and/or loops so as to improve affinity for G4s as well as the selectivity over duplex DNA. The G4 ligands approach is now considered to be a useful molecular tool to enhance and/or promote quadruplex-related biological effects in cells and shows high potential for future therapies.[20] To the best of our knowledge, however, very few studies have been devoted to the design of photo-reactive probes targeting G4s that could be interesting for phototherapy development. Freccero and co-workers have modified the well-known G4 ligand naphthalene diimide (NDI) with a phenol moiety that produced phenoxyl radicals upon irradiation.[21] They demonstrated the ability of this NDI-phenolate conjugate to kill MCF7 cancer cells after irradiation.

The design of new metal complexes targeting G-quadruplex DNA has attracted intense interest with regard to their potential anticancer properties.[22,23] Indeed, some Pt^{II},[24–28] Ni^{II},[29–31] Ru^{II},[32–34] and Ir^{III} complexes[35–37] have shown good affinity and selectivity towards G4s. In comparison to organic compounds, metal complexes have many advantages, such as a net positive charge, tunable geometry, and, most interestingly, some of them display potentially useful photochemical properties. In this context, polyazaaromatic ruthenium(II) complexes represent ideal candidates to target genetic material such as G4s. By virtue of their optical properties, including a large Stokes shift, good photostability, high quantum yield, and long-lived luminescence, they have been developed to probe different DNA sequences,[38] such as mismatches,[39] abasic sites,[40] or G4s.[32] More recently, two ruthenium(II) complexes, $[Ru(phen)_2(dph)]^{2+}$ and $[\{Ru(phen)_2\}_2(dph)]^{4+}$, based on the dph ligand (dph = dipyrazino[2,3-*a*:2′,3′-*h*]phenazine), have been reported to show good selectivity towards G4s.[41] However, none of the reported compounds is able to photo-induce oxidative damage under light irradiation. Highly π-deficient ligands, such as 1,4,5,8-tetraazaphenanthrene (TAP), are known to enhance the photo-oxidizing power of the resulting complexes.[42] Indeed, in the presence of DNA, photo-induced electron transfer (PET) from a guanine (G) base to the excited complex has been evidenced for ruthenium(II) complexes bearing at least two TAP ligands. This PET leads to dramatic consequences for living cells: (i) formation of an adduct between the complex and the guanine or (ii) DNA photo-cleavage (type I photo-oxidation).[43–45] A photoreaction process leading to bridging of two guanine bases of a quadruplex oligonucleotide by the rigid dinuclear complex $[(TAP)_2Ru(tpac)Ru(TAP)_2]^{4+}$ has also been reported.[46]

In the present study, three new photo-oxidizing ruthenium(II) complexes (Scheme 1) that selectively target G-quadruplex DNA over duplex DNA have been synthesized. They are based on the 2-(4-chlorophenyl)-1*H*-imidazo[4,5-*f*][1,10]phenanthroline (CPIP) ligand, some ruthenium(II),[47] platinum(II),[48] or iridium(III)[36] complexes of which have previously been reported for selective DNA switch. However, none of these complexes has shown an ability to induce photo-electron transfer (PET) with guanine units. With the aim of achieving this, the TAP moiety has been introduced in our ruthenium(II) complexes through different strategies (Scheme 1): (i) by incorporating two ancillary TAP ligands (complex **3**), (ii) by modifying the phenanthroline imidazole ligand with TAP (complex **2**), and (iii) by combining both strategies (complex **4**). Complex **1** bearing phen-based ligands was used as a reference. Steady-state luminescence, circular dichroism (CD), bio-layer interferometry (BLI), and surface plasmon resonance (SPR) studies have been performed, which demonstrated good affinity for G-quadruplex DNA as well as selectivity over duplex DNA. Preliminary biological studies with these complexes have been performed, which revealed that two of them showed remarkable photo-cytotoxicity towards U2OS osteosarcoma cells, whereas very low mortality was observed in the dark at the same photo-drug concentration.

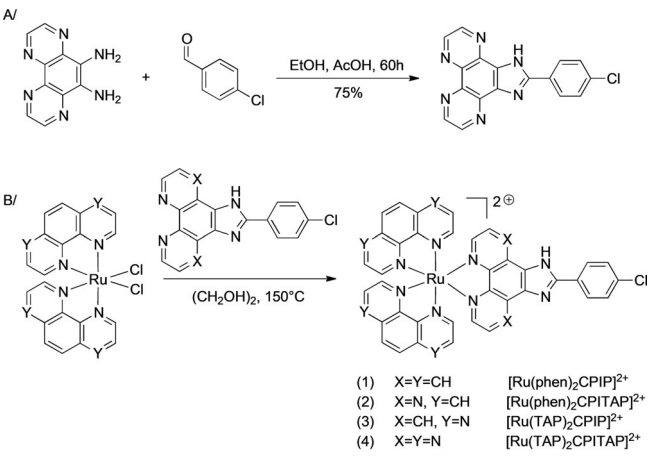

Scheme 1. Synthesis of A) CPITAP ligand and B) Ru^{II} complexes **1**–**4**.

Results and Discussion

Synthesis of complexes 1–4

The planar ligand CPIP (X = CH) was synthesized by condensation of 4-chlorobenzaldehyde with 1,10-phenanthroline-5,6-dione in an ammonium-containing medium as previously reported in the literature.[36] The ligand CPITAP (X = N) was obtained according to a new protocol developed in our laborato-

ry, using 4-chlorobenzaldehyde and 9,10-diamino-1,4,5,8-tetraazaphenanthrene. The reaction was carried out in a refluxing acetic acid/ethanol mixture over a period of 60 h. Purification by preparative chromatography on SiO_2 afforded pure CPITAP, which was characterized by ^1H and ^{13}C NMR spectroscopies and high-resolution mass spectrometry (HRMS) (see the Experimental Section and Figures S1, S2, and S11 in the Supporting Information). The corresponding Ru^{II} complexes were synthesized by direct chelation of the N^N ligand onto an Ru^{II} precursor bearing either 1,10-phenanthroline (phen, Y = CH) or 1,4,5,8-tetraazaphenanthrene (TAP, Y = N) moieties (Scheme 1). The reactions were carried out in the dark and under argon to avoid photo-dechelation and oxidation of the metal centre. Complexes **1**–**4** were characterized by ^1H NMR spectroscopy and HRMS analyses (see the Experimental Section and Figures S3–S10 and S12–S15) as well as UV/Vis, cyclic voltammetry (CV), and photochemical studies (see below).

Absorption and luminescence properties

The absorption and luminescence data for complexes **1**–**4** are gathered in Table 1 and in Figures S16–S19. For all of the complexes, the absorption bands in the UV region could be attributed to ligand-centred (LC) transitions from comparison with literature data, whereas the absorption maxima between 400 and 500 nm could be ascribed to metal-to-ligand charge-transfer (MLCT) transitions, as previously shown for similar complexes.[49,50] Emission spectra were measured at room temperature in acetonitrile and water, and at 77 K in EtOH/MeOH (4:1, v/v). Complexes **1**–**4** display broad unstructured emissions in both organic solvents and water.

Positive solvatochromism on going from acetonitrile to water and a hypsochromic shift of the emission band at 77 K suggest a more polar excited state with respect to the ground state, in agreement with the occurrence of charge transfer upon irradiation, that is, MLCT. The excited-state energy decreases on going from **1** with CPIP to **2** with more electron-withdrawing CPITAP, in agreement with stabilization of the LUMO localized on the imidazophenanthroline ligand. Similar observations were made for complexes **2**–**4**, whereby the increased number of π-deficient ligands results in stabilization of the metal-centred HOMO, leading to a more energetic transition. Comparison of luminescence lifetimes under air and under argon allows us to conclude that all of the complexes are capable of photosensitizing oxygen, as previously reported in the literature for similar compounds.[52,53] It is also noted that the luminescence quantum yield of complex **1** is lower in acetonitrile than in water, consistent with data for the complex $[Ru(phen)_3]^{2+}$.[54] The relatively low luminescence of complexes **2**–**4** in water is typical of TAP-based complexes and is generally attributed to increased non-radiative processes, likely due to interaction of the solvent with non-chelating nitrogen atoms (light-switch effect). It should also be noted that complex **4** showed a very short excited-state lifetime and a very low quantum yield of emission in water, thus suggesting poor photo-induced damaging properties.

Electrochemical study

The oxidation and reduction potentials of complexes **1**–**4** were determined by cyclic voltammetry measurements in dry deoxygenated acetonitrile (Table 2 and Figures S20–S23). Based on other similar Ru^{II} complexes described in the literature, we can assume that complexes **1**–**4** display a one-electron oxidation wave. This corresponds to the oxidation of Ru^{II} to Ru^{III}, as the anodic shift observed on going from **1** to **4** reflects stabiliza-

Table 2. Electrochemical data for complexes **1**–**4**.[a]

Complex	$E_{ox\ 1/2}$	E^*_{ox}[b]	$E_{red\ 1/2}$	E^*_{red}[b]
1	+1.37	−0.74	−1.30	+0.81
2	+1.63	−0.29	−0.77	+1.15
3	+1.83	−0.18	−0.78	+1.23
4	>2	>−0.16	−0.77	+1.39

[a] Data were measured at room temperature in MeCN with 0.1 M Bu_4NClO_4 as the supporting electrolyte (V vs. Ag/AgCl), concentration of complexes 0.8 mM. [b] Excited-state potentials estimated from the equations $E^*_{ox} = E_{1/2\ ox} - E_{0-0}$ and $E^*_{red} = E_{1/2\ red} + E_{0-0}$. The energy of the excited state, $E_{0\text{-}0}$, was estimated by Franck–Condon line-shape analysis of the emission spectrum at 298 K in CH_3CN (see the Supporting Information, Tables S1 and S2).

Table 1. Absorption and luminescence data for complexes **1**–**4**.

Complex	λ_{Abs} (ε)[a] CH_3CN	λ_{Em}[b] CH_3CN	H_2O	77 K	Φ_{Em}[c] CH_3CN	H_2O	τ [ns][d] CH_3CN	H_2O
1	460 (1.61)	597	603	570	0.009 (0.058)	0.069 (0.14)	115 (380)	572 (1315)
2	488 (0.59)	671	704	612	0.011 (0.082)	0.0059 (0.007)	376 (692)	162 (162)
3	471 (1.11)	623	641	598	0.037 (0.138)	0.017 (0.011)	686 (1620)	629 (786)
4	451 (1.28)	586	600	565	0.01 (0.02)	0.0006 (0.0005)	80 (78)	6 (6)

[a] λ in nm for the most bathochromic transition in MeCN (extinction coefficient, $\varepsilon \times 10^4\ M^{-1}cm^{-1}$). [b] λ in nm at RT in MeCN and H_2O and at 77 K in EtOH/MeOH (4:1, v/v). [c] Quantum yield of emission measured by comparison with the reference $[Ru(bpy)_3]^{2+}$, under air and under argon (in brackets), excitation at 450 nm, errors are estimated as 10%.[51] [d] Luminescence lifetime (after irradiation at $\lambda = 400$ nm) measured under air and under argon (in brackets); errors are estimated as 5%.

tion of the metal-centred HOMO due to the presence of highly π-deficient ligands (TAP), consistent with the spectroscopic properties. In the other direction, each complex displayed several one-electron reduction waves, corresponding to the successive addition of electrons to the ligands. The first reduction wave measured for **1** can be attributed to reduction of phen moieties of CPIP or the ancillary ligands. For complexes **2**–**4**, the first reduction wave, anodically shifted with respect to complex **1**, corresponds to reduction of the TAP moiety of either CPITAP or the ancillary ligand.

All of these data suggest the following photophysical scheme for this family of complexes. According to literature data and our results, we can safely conclude that the HOMO is metal-centred and that its relative energy depends on the respective ligands surrounding the metal. The more π-deficient ligands that are chelated to the metal centre, the less reducing the complex will be. As for the LUMO, it is centred on a ligand, confirming the MLCT nature of the excited state. From the cyclic voltammetry measurements and the spectroscopic data, the oxidation and reduction potentials of the excited state can be roughly estimated. Not surprisingly, complexes **3** and **4** display strong photo-oxidizing power (+1.23 and +1.39 V vs. Ag/AgCl, respectively). With these results in hand, we tested whether a photo-induced electron transfer (PET) would occur in the presence of the most reducing building block of the DNA G-quadruplex, that is, a guanine residue ($E_{ox} = +1.10$ V vs. Ag/AgCl).[55]

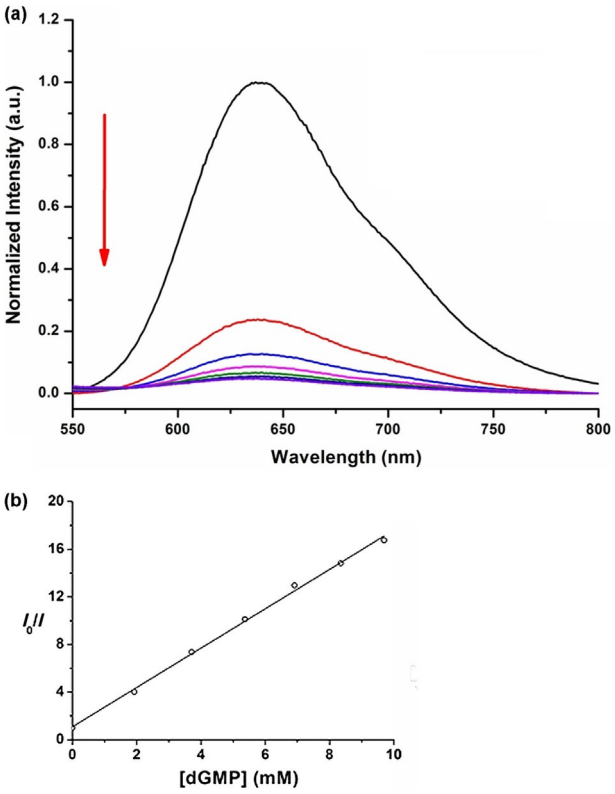

Figure 1. Luminescence quenching of complex **3** in the presence of dGMP: (a) emission spectra of complex **3** in the presence of increasing concentrations of dGMP; (b) Stern–Volmer plot. Complex concentration: 50 μM in Tris-HCl buffer (50 mM at pH 7.4). Addition of dGMP from 0 mM to 10 mM. Excitation at $\lambda = 430$ nm.

Luminescence studies in the presence of dGMP

As mentioned in the Introduction, G-quadruplex DNA is a guanine-rich sequence present in the genome. Recently, we have reported on a new family of Ru complexes exhibiting good affinity and selectivity towards G-quadruplex DNA.[41] However, these complexes proved not to be sufficiently oxidizing in their excited state to trigger direct oxidative damage (type I photoreactivity). Ruthenium(II) complexes bearing at least two TAP ligands are well known in the literature to photoreact with a guanine moiety upon irradiation. Therefore, the photoreactivities of our complexes towards dGMP were investigated by Stern–Volmer steady-state luminescence quenching experiments. As is well established in the literature, the luminescence quenching of an Ru^{II}-TAP complex upon addition of dGMP is due to electron transfer (ET) from dGMP to the complex in its excited state. According to their estimated E^*_{red} values (Table 2), complexes **1** and **2** should not be sufficiently photo-oxidizing to undergo ET with dGMP ($E_{ox} = +1.10$ V vs. Ag/AgCl). Indeed, as anticipated, no luminescence quenching was observed for these complexes in the presence of dGMP. In contrast, a Stern–Volmer plot obtained with complex **3** (Figure 1) showed luminescence quenching in the presence of increasing dGMP concentrations, with a high efficiency close to the diffusion limit (quenching rate constant $2.63 \times 10^9\ M^{-1}s^{-1}$). Based on thermodynamic data, this luminescence quenching can be safely ascribed to PET from the guanine moiety to the excited state of complex **3** [Eq. (1)].

$$[Ru]^{2+*} + G \rightarrow [Ru]^{1+} + G^{\bullet+} \quad (1)$$

Considering the oxidizing power of the excited state of **3** and using the empirical Rehm–Weller equation, it is expected that the process according to Equation (1) will be exergonic by about −0.13 eV. In the case of **4**, PET should also be favoured by about −0.29 eV, but the poor luminescence properties of this complex precluded luminescence quenching experiments.

Luminescence studies in the presence of ODNs

Due to the ability of complexes **1**–**3** to emit light in aqueous media, their luminescence upon the addition of increasing concentrations of oligonucleotides (ODNs) could be monitored. Experiments were performed with human telomeric wtTel23 ($^{3'}$TT(GGGATT)$_3$GGG$^{5'}$) and a GC-rich hairpin sequence ($^{3'}$(GC)$_4$TTTT(GC)$_4{}^{5'}$). The experiments were carried out in 10 mM HEPES (pH 7.4), 35 mM NaCl, 50 mM KCl buffer, in which the desired DNA structures (i.e., duplex or G-quadruplex) were formed (Figure S32). According to the redox properties of the complex, two behaviours were observed upon the addition of ODNs: (i) an increase in luminescence due to protection of the ruthenium(II) probe from the solvent in the hydrophobic environment of the ODN, or (ii) a decrease in luminescence due to PET with a neighbouring guanine base. Figure 2a,b show the

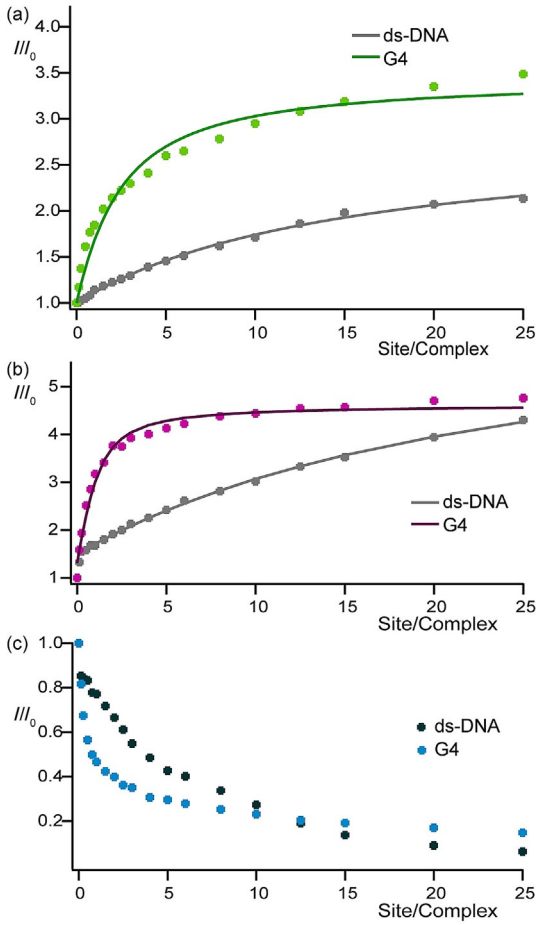

Figure 2. Luminescence titrations of complexes **1**–**3** with DNA. Luminescence titrations of complexes **1**, **2**, and **3** ((a), (b), and (c), respectively) were carried out in 10 mM HEPES (pH 7.4), 35 mM NaCl, 50 mM KCl buffer by adding increasing proportions of ds-DNA (GC-rich hairpin duplex $^{3'}(GC)_4TTTT(GC)_4^{5'}$, base pairs equivalents per Ru complex) or G-quadruplex DNA (wtTel23, $^{3'}TT(GGGATT)_3GGG^{5'}$, G-quartet equivalents per Ru complex). Solid lines were obtained by a modified McGhee–von Hippel fitting process (see the Supporting Information) to evaluate the binding affinities. Excitation at $\lambda = 450$ nm.

enhancement of the luminescence upon the addition of increasing amounts of wtTel23 or hairpin ODN for complexes **1** and **2**. This behaviour is consistent with (i) protection of the complex by the ODN, which decreases the rate of non-radiative processes, (ii) the fact that no luminescence quenching was observed in the presence of guanine moieties (see above). In contrast, the luminescence of complex **3** was quenched upon the addition of increasing amounts of DNA (Figure 2c), in accordance with PET and the Stern–Volmer plot.

The above results from steady-state luminescence studies with **1**–**3** suggested a strong interaction between DNA and these complexes. We thus decided to further investigate the interactions of the complexes with DNA in order to evaluate whether they might display a specific affinity towards G-quadruplex structures over double-stranded DNA.

DNA binding analysis

Various biophysical techniques, including FRET melting, UV/Vis spectrophotometry, circular dichroism (CD), NMR, and SPR have been developed for studying G-quadruplex DNA/ligand interactions.[17] In the present case, the use of UV/Vis absorbance was found to be unsuitable for determining the binding affinity. Modifications of the absorption spectra of the complexes were detected upon the addition of increasing concentrations of G-quadruplex DNA (Figures S24–S31), but they were relatively moderate and thus it was tedious to measure a binding affinity. Binding affinities of complexes **1** and **2** for G-quadruplex and duplex DNA could also be estimated by fitting the variation in luminescence intensity with the ratio of binding sites per complex (Figure 2). Complex **1** showed apparent dissociation constants (K_D) of 77 μM for duplex DNA and 6.5 μM for G-quadruplex DNA. The difference in binding affinities for duplex and G-quadruplex DNA was more drastic for complex **2**, with K_D values of 123 μM and 2 μM, respectively. Only qualitative conclusions can be made about the affinity of complex **3** for wtTel23 G-quadruplex versus GC-rich hairpin DNA, since a dynamic quenching process is also operative, which should alter the luminescence intensity. However, it can be observed that the slope of the curve is steeper with G-quadruplex DNA than with duplex DNA, indicating that the binding affinity is certainly stronger for the former. We thus evaluated the affinities of these complexes towards DNA by means of CD melting assays, BLI, and SPR.

CD melting assays

The ability of complexes **1**–**4** to interact with G-quadruplex DNA was first investigated through CD experiments. CD analyses were carried out in 10 mM Tris-HCl, 100 mM NaCl, or 100 mM KCl buffer. As anticipated, in buffer containing 100 mM NaCl, wtTel23 folded into an antiparallel topology characterized by two positive peaks at 242 and 294 nm, respectively, and a negative peak at 262 nm (Figure S33). Upon addition of complexes **2**–**4**, minor changes in the ellipticity of wtTel23 were observed, suggesting that these complexes did not induce major structural changes in the antiparallel conformation of the G-quadruplex DNA (Figure S33). For complex **1**, we also observed the appearance of a shoulder at 270 nm, attributable to a slight modification of the topology induced by this complex (presence of hybrid II-type G4 folding). In buffer containing 100 mM KCl, wtTel23 folded into a hybrid II-type G4 structure, characterized by a maximum at 290 nm and a shoulder at 270 nm (Figure S34). Again, a minor change in the ellipticity of wtTel23 was observed, thus revealing no major structural changes upon binding. The duplex structure ($^{5'}CGT_3CGT_5ACGA_3CG^{3'}$ hairpin) was not affected as no change in the CD spectrum was observed upon addition of complexes **1**–**4** (Figure S35).

Next, we performed CD melting assays to evaluate whether complexes **1**–**4** exerted stabilizing or destabilizing effects on the G-quadruplex and hairpin duplex DNA structures. CD melting curves were recorded in the absence or presence of each

complex (at 5:1 complex/DNA ratio) in buffer containing 100 mM NaCl or 100 mM KCl (Table 3 and Figures S36 and S37) in the case of wtTel23 and in buffer containing 100 mM NaCl for hairpin duplex (Table 3 and Figure S38). The results of CD

Table 3. Melting temperatures (T_m) of wtTel23 and duplex hairpin in the absence or presence of ligands (5 equiv).[a]

	T_m [°C] (±1)	
Complex	wtTel23	hairpin
no complex	52.9 (61.9)	68.7
1	58.5 (76.0)	58.0
2	58.0 (64.0)	67.6
3	57.3 (67.0)	68.1
4	52.9 (61.9)	67.2

[a] WtTel23 sequence $^{3'}$TT(GGGATT)$_3$GGG$^{5'}$ was first annealed by heating at 95 °C for 5 min in Tris-HCl buffer (10 mM, pH 7.04) with 100 mM NaCl or 100 mM KCl (in brackets) and then allowed to cool to room temperature overnight. Oligonucleotide concentration 2.5 μM. Hairpin sequence $^{5'}$CGT$_3$CGT$_5$ACGA$_3$CG$^{3'}$ was first annealed by heating at 95 °C for 5 min in Tris-HCl buffer (10 mM, pH 7.04) with 100 mM NaCl and then allowed to cool to room temperature overnight. The ellipticity was recorded at 290 and 252 nm for wtTel23 and duplex hairpin, respectively.

melting experiments clearly showed that complexes **1**–**3** induced a slight stabilization of wtTel23, whereas none of the complexes significantly affected the stability of duplex DNA structures. The melting temperature assays thus confirmed the ability of most of the investigated complexes to selectively interact with G-quadruplex DNA over duplex DNA. It should be mentioned that each complex is a racemic mixture of two enantiomers and that preferential binding or a different binding mode of each enantiomer could arise. However, separation of the respective enantiomers represents a new and challenging task. Thus, we are presently unable to comment on whether the changes observed by CD are due to different binding modes of each enantiomer. Because this technique is not the most appropriate for direct measurements of affinity constants, we next performed BLI analysis, which allowed us to determine the thermodynamic parameters for the interaction.

Bio-layer interferometry studies

BLI is a label-free method for the measurement of affinity constants. It allows the determination of kinetic parameters of an interaction (such as SPR) and has been used to study biomolecular interactions between large biomolecules, such as protein–membrane interactions.[56] We have hitherto employed an SPR analysis method based on the use of a template-assembled synthetic G-quadruplex (TASQ) that allows precise control of G-quadruplex topology through the assembly of constrained structures on a template.[57–61] We have now adapted this SPR method for BLI. Different G-quadruplex features were used: intermolecular-like G-quadruplex motif **A** constrained in a parallel G-quadruplex topology, intramolecular G-quadruplex **B** (HTelo sequence in equilibrium between different topologies), human telomeric sequence (HTelo) **C** constrained in antiparallel topology, and hairpin DNA **D** (Figure 3). Each of the systems **A**–**C** formed the desired G-quadruplex structure under the conditions used for BLI analysis (10 mM HEPES pH 7.4, 35 mM NaCl, 50 mM KCl).[57,58]

Each evaluated complex showed K_D values in the micromolar range for G-quadruplex topologies **A**, **B**, and **C** (Table 4 and Figures S39–S42). These values fall within the range of those reported for related ruthenium(II) complexes interacting with G-quadruplexes. It is noteworthy that the substitution of carbon atoms by nitrogen atoms in the ligands (i.e., two phen ligands in **1** replaced by two TAP ligands in **3**; the CPIP ligand in **1** replaced by the CPITAP ligand in **2**) only weakly affects the interaction with G-quadruplex DNA. More interestingly, each ruthenium(II) complex showed a higher affinity for G-quadruplex structures than for duplex DNA. Indeed, it was impossible to measure K_D values for interaction with duplex system **D** within the concentration range used in this study (i.e., from 5 to 40 μM), which were presumably higher than 1 mM for each complex. The good selectivity was further confirmed by SPR analysis using systems **B** and **D**. We obtained K_D values for the G-quadruplex system **B** of the same order of magnitude as from BLI analysis, whereas none of the complexes showed an affinity with duplex DNA **D** within the concentration range used (Figure S43 and Table S3).

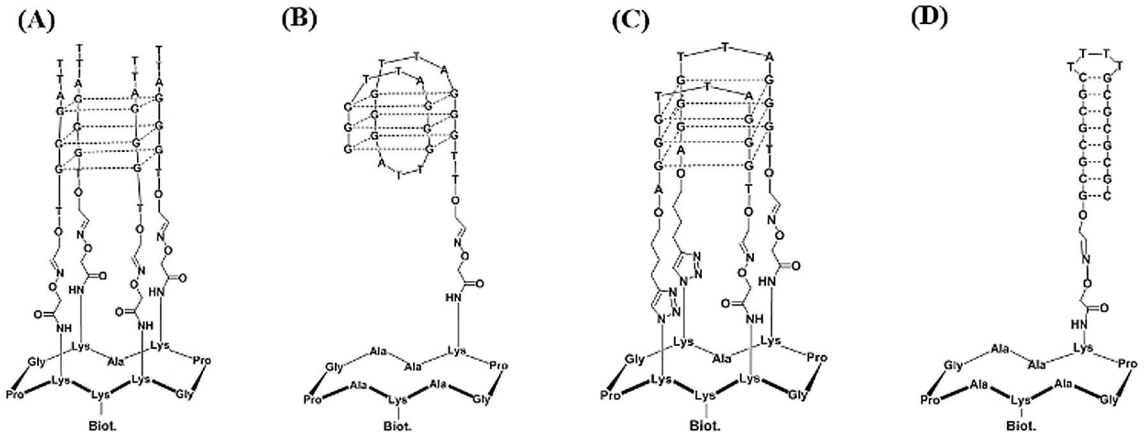

Figure 3. G-quadruplex systems **A**–**C** and duplex control **D** used for bio-layer interferometry studies: (**A**) parallel-stranded quadruplex (intermolecular-like G-quadruplex), (**B**) intra quadruplex (intramolecular-like G-quadruplex), (**C**) antiparallel human telomeric sequence, and (**D**) duplex (hairpin).

Table 4. Data for the interactions of complexes **1**–**4** with DNA structures **A**–**D** from BLI analyses.

DNA structure	Constants	Complex 1	2	3	4
A	k_{on} (10^3 M^{-1} s^{-1})	2.2 ± 1.3	9.4 ± 1.4	27 ± 1.2	8.0 ± 2.1
	k_{off} (10^{-1} s^{-1})	1.8 ± 0.5	2.9 ± 0.3	3.7 ± 0.6	13 ± 0.2
	K_D (μM)[a]	80 ± 20	31 ± 8	20 ± 11	182 ± 74
B	k_{on} (10^3 M^{-1} s^{-1})	5.9 ± 1.6	130 ± 0.1	100 ± 1.0	27 ± 1.3
	k_{off} (10^{-1} s^{-1})	0.37 ± 0.8	1.5 ± 0.1	1.5 ± 1.4	4.6 ± 3.0
	K_D (μM)[a]	6.0 ± 4.0	1.0 ± 0.5	2.0 ± 0.5	22 ± 10
C	k_{on} (10^3 M^{-1} s^{-1})	22 ± 1.0	62 ± 1.2	280 ± 1.6	61 ± 1.7
	k_{off} (10^{-1} s^{-1})	1.6 ± 0.4	1.8 ± 0.1	2.4 ± 0.8	9.4 ± 1.6
	K_D (μM)[a]	8.0 ± 2.0	3.0 ± 0.5	1.0 ± 1	10 ± 8
D	k_{on} (10^3 M^{-1} s^{-1})	n.d.[b]	n.d.[b]	n.d.[b]	n.d.[b]
	k_{off} (10^{-1} s^{-1})	n.d.[b]	n.d.[b]	n.d.[b]	n.d.[b]
	K_D (μM)[a]	n.d.[b]	n.d.[b]	n.d.[b]	n.d.[b]

[a] Equilibrium dissociation constants deduced from the kinetic rate constants. [b] Due to very low binding of the different complexes with hairpin DNA, the kinetics of the interactions could not be determined (n.d.) in the studied concentration range. This was confirmed by SPR analysis (Figure S43). Running buffer: 10 mM HEPES pH 7.4, 35 mM NaCl, 50 mM KCl.

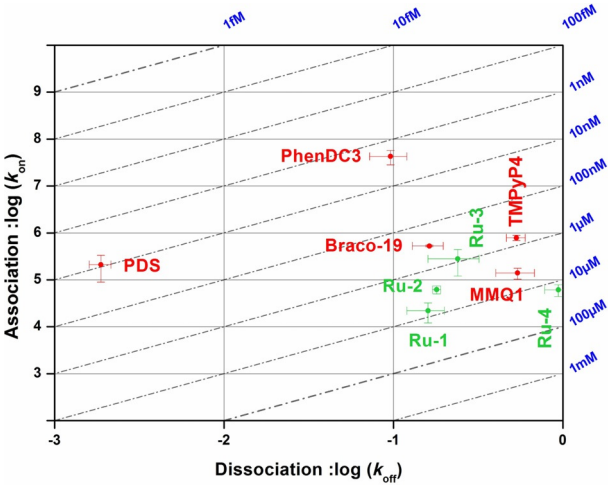

Figure 4. Isoaffinity plot and kinetic characterization for G-quadruplex structure **C**. For PhenDC$_3$, BRACO-19, MMQ$_1$, and TMPyP$_4$ (in red), the analyses were performed by SPR;[61] for ruthenium(II) complexes (in green), data are from BLI analysis. K_D (parallel diagonal lines), k_{on} (association kinetic constant, *y*-axis), k_{off} (dissociation kinetic constant, *x*-axis).

It was also noticed that the affinities of complexes **1**–**4** were higher for G-quadruplex structures **B** and **C**, which contain TTA loops, than for parallel-stranded quadruplex **A**. This is consistent with interactions of the complexes with G-quadruplexes through mixed π-stacking over the guanine tetrad and further interactions with loops and grooves (see the Molecular Modelling section below). To obtain further information on the affinity of complexes **1**–**4** for G-quadruplex DNA, the association (k_{on}) and dissociation (k_{off}) constants of the interaction were determined (Table 4), which again revealed the relatively minor influence of the replacement of carbon by nitrogen atoms in complexes **1**–**4**. Indeed, for a given G-quadruplex structure, k_{on} and k_{off} differ only slightly.

For the most biologically relevant G-quadruplex structure **C**, k_{on} and k_{off} values were also compared with those of well-known compounds that interact with G-quadruplex DNA (i.e., pyridostatine PDS, Phen-DC3, BRACO-19, MMQ1, and TMPyP4).[61]

As illustrated in Figure 4, complexes **1**–**4** display association and dissociation rates that are similar to those of BRACO, MMQ1, and TMPyP4. In particular, the fact that our complexes showed similar affinity to BRACO-19, which has demonstrated anticancer activity through the stabilization of G-quadruplex at the telomere,[62] prompted us to study their phototoxicity.

Molecular modelling

To obtain further insights into the interactions with G-quadruplex DNA, molecular docking calculations were carried out. The most interesting complex **3** (due to its photophysical properties) was docked to the human telomeric DNA structure (PDB entry 1KF1, wtTel23 in parallel conformation). From analysis of the best-ranked docked positions, two binding modes were obtained (Figure 5). The first involved a π-stacked positioning of **3** over the guanine tetrad, while the second involved insertion of the complex into the TTA loop of the G-quadruplex through the CPIP ligand. Initial calculations were performed with the Δ-isomer of complex **3** to afford the two best-ranked positions in Figure 5. However, similar docked positions were obtained with the other Λ-enantiomer (see Figure S44 in the Supporting Information).

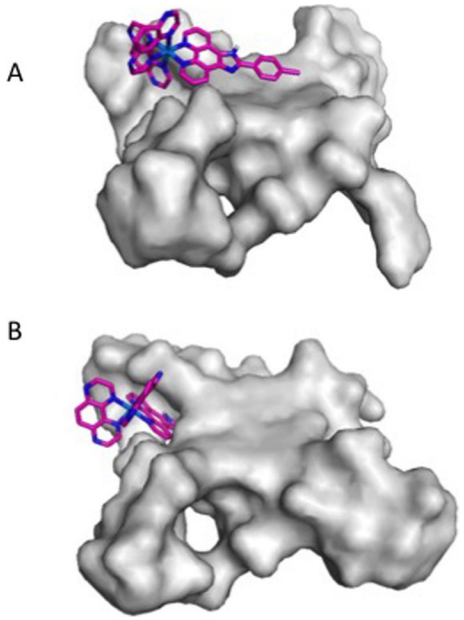

Figure 5. Molecular modelling of the interactions of complex **3** (Δ-isomer) with G-quadruplex DNA. Docking calculations for interaction of complex **3** with G-quadruplex human telomeric DNA structure (PDB entry 1KF1): (**A**) in π-stacked position over the guanine tetrad, (**B**) interaction with TTA loop.

Dynamic molecular mechanics simulations were then carried out in order to assess the stabilities of these two docking positions. In both cases, the complex remained tightly bound in its

relative position (either in interaction with the TTA loop or π-stacked) for up to 20 ns, thus emphasizing the strong affinity displayed by **3** towards G-quadruplex DNA. These results are consistent with those of the BLI experiments. Indeed, the affinity of complex **3** towards structure **A** (i.e., without a loop) is lower than those towards structures with a loop ($K_D = 20$ μM for **A**; $K_D \approx 2$ μM for **B** and **C**), confirming the importance of the second docked position (i.e., loop interactions).

Cell penetration

By virtue of the ability of complex **1** to emit light in aqueous media, its penetration into U2OS osteosarcoma cells could be studied by confocal microscopy.[63] Cells were incubated with 20 μM complex **1** for 24 h. As shown in Figure 6, complex **1** showed efficient penetration into the cells, including in the nuclei.

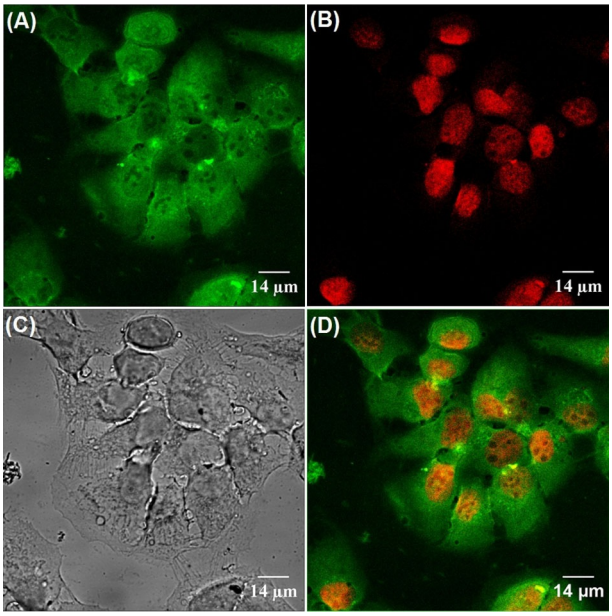

Figure 6. Cell penetration study. Fluorescence microscopy images of U2OS cells after incubation with 20 μM of complex **1** for 24 h, DMEM buffer: (**A**) Ru^{II} complex in green, (**B**) the nuclei in red, stained by Draq5; (**C**) bright-field and (**D**) merged image. Scale bar 14 μm.

Photo-cytotoxicity

Preliminary photo-cytotoxicity studies were performed with complexes **1**–**4** on U2OS osteosarcoma cells. Figure 7 depicts the percentage of metabolically active cells after incubation with 10 μM of complexes **1**–**4** for 24 h and subsequent irradiation for 30 min (orange bars). Non-irradiated controls were also performed (blue bars). Interestingly, non-irradiated cells displayed very low rates of mortality, whereas irradiation of the cells led to a dramatic decrease in survival. Indeed, 100% mortality was obtained at 10 μM for complexes **1** and **3**, whereas complex **2** was slightly less efficient, inducing 70% mortality. As anticipated, complex **4** showed only very weak phototoxicity in comparison with non-irradiated control cells. The strong

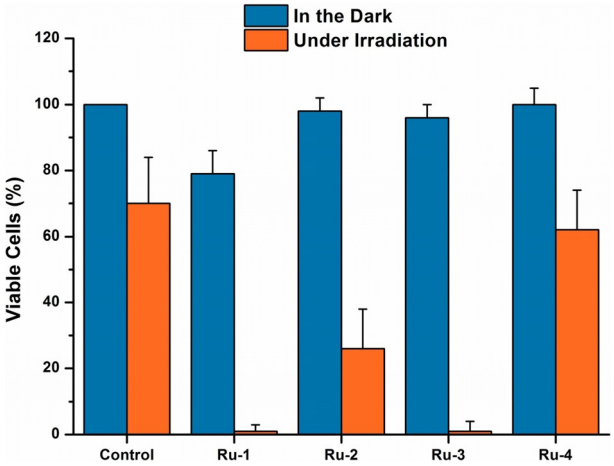

Figure 7. Cell viability studies. Percentage of viable U2OS cells after incubation with complexes **1**–**4** for 24 h in the dark followed by 30 min of irradiation (orange bars) or not irradiated (blue bars). The tetrazolium salt-based WST-1 assay was performed 24 h after irradiation. Values were normalized to untreated and non-irradiated U2OS cells. Error bars indicate SD.

phototoxicity of complex **3** was confirmed by microscopic observation of the cells, as revealed by tetrazolium salt-based metabolic assay, which revealed extensive cell death upon irradiation (dead cells can clearly be recognized by a change in shape, see Figure S45).

A possible explanation for the phototoxicity of **1**–**3** is that the internalized ruthenium complexes react with the biological material through a type I photoreaction (i.e., photoelectron transfer) or type II photoreaction (singlet oxygen photosensitization), both mechanisms being likely to induce DNA damage, ultimately leading to cell death. On the contrary, the low photo-cytotoxicity of **4** most likely originates from its short excited-state lifetime, resulting in a poor photo-damaging ability.

Conclusions

A series of new ruthenium(II) complexes has been designed to target and photoreact with G-quadruplex DNA through incorporation of the CPIP ligand (or similar). As anticipated, the photophysical properties of these complexes are consistent with MLCT transitions and a metal-centred HOMO. Consequently, these complexes are able to react with DNA through type II photoreaction (i.e., formation of singlet oxygen) or through photo-induced charge transfer (PET). All four designed complexes **1**–**4** displayed a good affinity for G-quadruplex DNA and selectivity over duplex DNA. Docking studies and molecular dynamic simulations revealed that this affinity is due to π-π stacking above the tetrad and interaction with the TTA loop.

Strikingly, both complexes **1** and **3** elicited a dramatic photo-cytotoxic effect, as 100% mortality was obtained upon irradiation of U2OS osteosarcoma cells in their presence, whereas very low mortality was observed in the dark at the same drug concentration. Further studies are underway with the aim of establishing whether this photo-cytotoxic effect is mainly due to a type II photoreaction (i.e., singlet oxygen pho-

tosensitization) or a type I photoreaction (i.e., photo-induced charged transfer (PIET)). Further experiments are currently being performed to investigate whether telomeric DNA damage is induced in cells by complexes **1** and **3**. Interestingly, this photo-cytotoxicity should not involve the inhibition of telomerase activity through the stabilization of G-quadruplex DNA as U2OS osteosarcoma cells do not express the telomerase enzyme. To the best of our knowledge, this would be the first example of high photo-cytotoxicity based on the use of metal complexes targeting telomeric DNA, through a mechanism that does not involve the inhibition of telomerase. Therefore, the photo-cytotoxicity of these two complexes will also be comparatively evaluated towards both telomerase-expressing cancer cells and normal non-immortalized cells.

Experimental Section

Material and methods

$[Ru(phen)_2Cl_2]$,[64] $[Ru(TAP)_2Cl_2]$,[42] 1,10-phenanthroline-5,6-dione,[65] 9,10-diamino-1,4,5,8-tetraazaphenanthrene,[65] and 2-(4-chlorophenyl)-1*H*-imidazo[4,5-*f*][1,10]phenanthroline (CPIP)[48] were synthesized according to previously described literature protocols. The oligonucleotides wtTel23 ($^{3'}$TT(GGGATT)$_3$GGG$^{5'}$), GC-rich hairpin duplex ($^{3'}$(GC)$_4$TTTT(GC)$_4^{5'}$), and hairpin duplex sequence $^{5'}$CGT$_3$CGT$_5$ACGA$_3$CG$^{3'}$ were prepared by standard automated solid-phase oligonucleotide synthesis on a 3400 DNA synthesizer. After purification by RP-HPLC, they were thoroughly desalted by size-exclusion chromatography (SEC). All solvents and reagents for the synthesis were of reagent grade and were used without any further purification. All solvents for the spectroscopic and electrochemical measurements were of spectroscopic grade. Water was purified with a Millipore Milli-Q system. ^{1}H and ^{13}C NMR spectra were measured from solutions in $CDCl_3$ or CD_3CN on a Bruker AC-300 Avance II (300 MHz) or a Bruker AM-500 (500 MHz) spectrometer at 20 °C. Chemical shifts (in ppm) were referenced to the residual peak of the solvent as an internal standard. High-resolution mass spectra (HRMS) were recorded on a Q-extractive Orbitrap spectrometer from Thermo-Fisher, using reserpine as an internal standard. Samples were ionized by electrospray ionization (ESI; capillary temperature 320 °C, vaporizer temperature 320 °C, sheath gas flow rate 5 mL min^{-1}).

Synthesis

2-(4-Chlorophenyl)-1*H*-imidazo[4,5-*f*]pyrazino[2,3-*h*]quinoxaline (CPITAP): A solution of 9,10-diamino-1,4,5,8-tetraazaphenanthrene (53 mg, 0.250 mmol) and 2-(4-chlorophenyl)-1*H*-imidazo[4,5-*f*][1,10]phenanthroline (35 mg, 0.250 mmol) in EtOH (2.5 mL) was heated under reflux for 24 h. AcOH (3 mL) was then added and the mixture was heated at 110 °C for 60 h. After cooling, the AcOH was evaporated under vacuum. The crude dark-green solid was then purified by preparative chromatography on SiO_2 ($CHCl_3$/EtOH, 99:1) to afford pure CPITAP as a yellow powder (62 mg, 75%). ^{1}H NMR (300 MHz, $CDCl_3$): $\delta = 9.13$ (d, 2H, $J = 1.8$ Hz), 9.06 (d, 2H, $J = 2.0$ Hz), 8.24 (d, 2H, $J = 8.6$ Hz), 7.52 ppm (d, 2H, $J = 8.6$ Hz); ^{13}C NMR (75 MHz, $CDCl_3$): $\delta = 151.71$, 151.70, 145.73, 145.72, 143.79, 139.52, 137.6, 129.63, 129.62, 128.13 ppm; HR-MS: calcd for $C_{17}H_{10}N_6Cl$: 333.06500 Da; found 333.06489 Da.

$[Ru(phen)_2CPIP]\cdot 2PF_6$ (1): $[Ru(phen)_2Cl_2]$ (20 mg, 0.037 mmol) and CPIP (15 mg, 0.045 mmol) were dissolved in ethylene glycol (3 mL) and the solution was heated at 120 °C for 20 h in the dark under argon. After cooling and addition of aqueous NH_4PF_6 solution, a solid was formed. The latter was collected by filtration and washed three times each with water, EtOH, and Et_2O to afford the final pure product as an orange powder (36 mg, 90%). ^{1}H NMR (500 MHz, CD_3CN): $\delta = 9.05$ (d, 1H, $J = 8.2$ Hz), 8.89 (d, 1H, $J = 8.4$ Hz), 8.59 (dd, 4H, $J = 8.3$ Hz, $J = 1.2$ Hz), 8.28 (d, 2H, $J = 8.7$ Hz), 8.25 (s, 4H), 8.07 (dd, 2H, $J = 10.5$ Hz, $J = 4.8$ Hz), 8.01 (d, 2H, $J = 5.4$ Hz), 7.96 (d, 2H, $J = 5.2$ Hz), 7.67–7.59 ppm (m, 8H); HR-MS: calcd for $C_{43}H_{27}N_8ClF_6PRu$ (**1**$-1PF_6$): 931.07595 Da; found 931.07688 Da.

$[Ru(phen)_2CPITAP]\cdot 2PF_6$ (2): $[Ru(phen)_2Cl_2]$ (20 mg, 0.037 mmol) and CPITAP (15 mg, 0.044 mmol) were dissolved in ethylene glycol (3 mL) and the solution was heated at 120 °C for 20 h in the dark under argon. After cooling and addition of aqueous NH_4PF_6 solution, a solid was formed. The latter was collected by filtration and washed three times each with water, EtOH, and Et_2O to afford the crude product. Purification by preparative chromatography on SiO_2 ($CH_3CN/H_2O/NH_4Cl_{(sat)}$, 4:4:1, v/v/v) gave the final product as a red powder (18 mg, 64%). ^{1}H NMR (500 MHz, CD_3CN): $\delta = 8.86$ (d, 2H, $J = 2.9$ Hz), 8.65 (d, 4H, $J = 8.3$ Hz), 8.31 (d, 2H, $J = 8.8$ Hz), 8.28 (s, 4H), 8.13 (d, 2H, $J = 5.0$ Hz), 8.08 (d, 2H, $J = 2.9$ Hz), 8.00 (d, 2H, $J = 4.8$ Hz), 7.69–7.62 ppm (m, 6H); HR-MS: calcd for $C_{41}H_{25}N_{10}ClRu$ (**2**$-2PF_6$): 394.05086 Da; found 394.05131 Da.

$[Ru(TAP)_2CPIP]\cdot 2PF_6$ (3): $[Ru(TAP)_2Cl_2]$ (20 mg, 0.037 mmol) and CPIP (15 mg, 0.045 mmol) were dissolved in ethylene glycol (3 mL) and the solution was heated at 120 °C for 20 h in the dark under argon. After cooling and addition of aqueous NH_4PF_6 solution, a solid was formed. The latter was collected by filtration and washed three times each with water, EtOH, and Et_2O to afford the final pure product as an orange powder (34 mg, 83%). ^{1}H NMR (500 MHz, CD_3CN): $\delta = 9.01$–8.94 (m, 6H), 8.62 (s, 4H), 8.27 (d, 2H, $J = 8.6$ Hz), 8.24 (d, 2H, $J = 2.8$ Hz), 8.19 (d, 2H, $J = 2.7$ Hz), 8.04 (d, 2H, $J = 4.3$ Hz), 7.73 (dd, 2H, $J = 8.3$ Hz, $J = 5.3$ Hz), 7.66 ppm (d, 2H, $J = 8.6$ Hz); HR-MS: calcd for $C_{39}H_{23}N_{12}ClF_6PRu$ (**3**$-1PF_6$): 941.053699 Da; found: 941.054467 Da.

$[Ru(TAP)_2CPITAP]\cdot 2PF_6$ (4): $[Ru(TAP)_2Cl_2]$ (20 mg, 0.037 mmol) and CPITAP (15 mg, 0.044 mmol) were dissolved in ethylene glycol (3 mL) and the solution was heated at 120 °C for 20 h in the dark under argon. After cooling and addition of aqueous NH_4PF_6 solution, a solid was formed. The latter was collected by filtration and washed three times each with water, EtOH, and Et_2O to afford the crude product. Purification by preparative chromatography on SiO_2 ($CH_3CN/H_2O/KNO_{3(sat)}$, 7:2:1, v/v/v) gave the final product as a red powder (10 mg, 25%). ^{1}H NMR (500 MHz, CD_3CN): $\delta = 9.01$–8.98 (m, 4H), 8.97 (d, 2H, $J = 2.8$ Hz), 8.64 (s, 4H), 8.32 (d, 2H, $J = 8.6$ Hz), 8.29 (s, 2H), 8.24 (d, 2H, $J = 2.7$ Hz), 8.15 (d, 2H, $J = 2.8$ Hz), 7.66 ppm (d, 2H, $J = 8.5$ Hz); HR-MS; calcd for $C_{37}H_{21}N_{14}ClRu$ (**4**$-2PF_6$): 396.04136 Da; found: 396.04171 Da.

Absorption and luminescence studies

UV/Vis absorption spectra were recorded on a Shimadzu UV-1700 spectrophotometer. The concentration of the complexes was 50 μM. Room temperature luminescence spectra were recorded on a Varian Cary Eclipse instrument. Luminescence intensity at 77 K was recorded on a FluoroLog 3 FL3-22 from Jobin Yvon equipped with an 18 V 450 W short-arc xenon lamp and an R928P photomultiplier, using an Oxford Instruments Optistat DN nitrogen cryostat controlled by an Oxford Intelligent Temperature Controller (ITC503S). Quantum yields were obtained using $[Ru(bpy)_3]^{2+}$ as a reference.[51] Luminescence lifetime measurements were performed after irradiation at $\lambda = 400$ nm obtained as the second harmonic of a titanium:sapphire laser (picosecond Tsunami laser Spectra Physics

3950-M1BB + 39868-03 pulse picker doubler) at a repetition rate of 80 kHz. A Fluotime 200 instrument from AMS Technologies was used for the decay acquisition. It consists of a GaAs microchannel plate photomultiplier tube (Hamamatsu model R3809U-50) followed by a time-correlated single-photon counting system from Picoquant (PicoHarp300). The ultimate time resolution of the system is close to 30 ps. Luminescence decays were analysed with FLUOFIT software available from Picoquant.

Electrochemical studies

Cyclic voltammetry was carried out in a one-compartment cell, using a glassy carbon disk working electrode (approximate area 0.03 cm^2), a platinum wire counter electrode, and an Ag/AgCl reference electrode. The potential of the working electrode was controlled by an Autolab PGSTAT 100 potentiostat through a PC interface. Cyclic voltammograms were recorded at a sweep rate of 100 $mV s^{-1}$ from solutions in dry acetonitrile (Sigma–Aldrich, HPLC grade). The concentration of the complexes was 8×10^{-4} $mol L^{-1}$, with 0.1 $mol L^{-1}$ tetrabutylammonium perchlorate as supporting electrolyte. Before each measurement, the samples were purged with nitrogen. Redox potentials were determined by comparison with ferrocene, added at the end of the measurement.

Luminescence titration experiments of complexes **1**–**3** with dGMP were conducted with a Varian Cary Eclipse instrument. A solution of dGMP (5 mM) was progressively added to a solution of the respective complex (50 μM) in 50 mM Tris-HCl buffer, pH 7.4. Luminescence titration experiments with ODNs (GC-rich hairpin or wtTel23 G-quadruplex DNA) were conducted by recording spectra from solutions in 10 mM HEPES, 35 mM NaCl, 50 mM KCl (pH 7.4) buffer on a Varian Cary Eclipse instrument for complexes **1** and **3**, and on a FluoroLog 3 FL3-22 from Jobin Yvon for complex **2**. Titrations were performed by starting from the highest DNA concentration (10 μM) and progressively decreasing it, whilst the concentration of the complex (5 μM) was kept constant. Fitting equations are described in the Supporting Information.

CD experiments

Prior to CD analysis, oligonucleotides were annealed by heating at 95 °C for 5 min in buffered medium, then allowed to cool to room temperature overnight. Spectra were recorded on a JASCO J-810 spectropolarimeter from solutions in 1 cm pathlength quartz cuvettes at 5 °C increments from 25 °C to 90 °C over the wavelength range from 220 to 330 nm. At each temperature, the spectrum was an average of three scans with response time 0.5 s, data pitch 1 nm, bandwidth 4 nm, and scanning speed 200 $nm min^{-1}$. For CD melting experiments, the ellipticity was recorded at 290 and 252 nm for wtTel23 and duplex hairpin, respectively. Melting temperatures were obtained through Boltzmann fitting with Origin software. Each curve fit was only accepted with $r > 0.99$.

Bio-layer interferometry (BLI)

BLI sensors coated with streptavidin (SA sensors) were purchased from Forte Bio (PALL). Prior to functionalization, they were immersed for 10 min in buffer to dissolve the sucrose layer. They were then dipped for 15 min in the requisite DNA solution (biotinylated systems **A**–**D**) at 100 nM and rinsed in buffer solution (10 mM HEPES pH 7.4, 35 mM NaCl, 50 mM KCl, and 0.5% v/v surfactant P_{20}) for 10 min. The functionalized sensors were next dipped in solutions of the respective ruthenium complexes at different concentrations (see the Supporting Information) for 2 min interspersed by a rinsing step in the buffer solution for 4 min. Reference sensors without DNA immobilization were used to subtract the non-specific adsorption on the SA layer. The sensorgrams were fitted using a heterogeneous model (see the sensorgrams in Figures S39–S42). The reported values are the means of representative independent experiments, and the errors provided are standard deviations from the mean. Each experiment was repeated at least twice.

Computational studies

Docking experiments were performed with complex **3**, the geometry of which was first optimized at the B3LYP/6-31 g* level using Gaussian 09 software. The AutoDock 4.0 software package was then used on the crystal structure of parallel quadruplexes from human telomeric DNA (PDB entry: 1KF1). A grid of $80\times80\times80$ points with a spacing of 0.5 Å between these points was used; non-polar hydrogen atoms were merged and Gasteiger–Hückel charges were added on both the complex and the G-quadruplex. The parameters for the Ru atom were set at $r = 2.96$ Å, $q = +2.0$ and the van der Waals well depth was 0.056 $kcal mol^{-1}$. The docking calculations involved a genetic algorithm search generating 100 docked structures. A default protocol was applied, with an initial population of 150 randomly placed individuals, a maximum number of 2.5×10^5 energy evaluations, a maximum number of 2.7×10^4 generations, a mutation rate of 0.02, and a crossover rate of 0.8. Results differing by less than 2 Å in positional root-mean-square deviation (RMSD) were clustered together and represented the result with the most favourable free binding energy. Regarding the dynamic molecular mechanics simulation, the AMBER 12 software package was chosen and applied to the two best-ranked positions obtained from the docking calculations. The complex was broken down into its constituent ligands and their specific parameters were generated with the ANTECHAMBER module and the GAFF force field, whereas charges were calculated through an RESP fitting of HF/6-31g*-level calculations. The docking structures were solvated in a TIP3P water box, the dimensions of which were set at least 10 Å larger than the solute in every direction. Sodium cations were added until the global charge was neutral and long-range electrostatic interactions were computed using the particle-mesh Ewald method with a cut-off value of 10 Å. After minimization and heating, an MD simulation was run at 300 K for 20 ns with the time step set at 1 fs.

Confocal laser scanning microscopy

U2OS cells were grown at 37 °C in a humidified atmosphere with 5% CO_2 in DMEM medium (Westburg) containing 10% foetal bovine serum (FBS) (Gibco) and 1% penicillin/streptomycin (Westburg). 20000 cells were seeded onto a coated microscope slide and incubated with 20 μM of complex **1** for 24 h in the dark. After incubation, the medium containing the complex was removed, and fresh medium was added to the cells. The cells were rinsed in pre-warmed PBS, fixed in 4% paraformaldehyde (VWR) for 10 min, and labelled with Draq5 (eBioscience) following the instructions of the manufacturer. A confocal laser scanning microscopy system (Zeiss LSM 710) was used to acquire the images, which were processed with Zen software.

Photocytotoxicity experiments

U2OS cells were cultured for 24 h in DMEM (Westburg) containing 10% FBS (Gibco) and 1% penicillin/streptomycin (Westburg) in 96-well plates to reach a density of 10000 cells/well. The supernatant was then removed and fresh medium containing 10 μM of the

requisite complex was added. After 24 h of incubation at 37 °C in the dark, cells were rinsed twice with PBS to remove non-internalized complex. They were then illuminated for 30 min with blue LEDs (LED strip IP68 60 LED m^{-1} from Prolumia, 405 nm at 15.7 W m^{-2}). The distance between the light source and the culture plate was 10 cm. Cultures were rinsed with PBS and then illuminated in PBS to avoid absorption by coloured culture medium. Plates serving as a dark control were protected from illumination with aluminium foil. Illuminated and control cultures were immediately returned to the incubator at 37 °C in a humidified environment and cultured in fresh medium for an additional 24 h. The cell viability was measured 1 day post-irradiation using 10 μL/well of WST-1 reagent (Sigma–Aldrich) following the manufacturer's instructions. The ratio of the optical density at $\lambda = 450$ nm under each set of conditions to that of control cells (non-transfected and non-irradiated, 100% viability) was used to determine the relative viability. These measurements were performed twelve times.

Acknowledgements

J.W., M.A., L.M., and B.E. gratefully acknowledge the Fonds National pour la Recherche Scientifique (F.R.S.-FNRS), the Fonds pour la Formation à la Recherche dans l'Industrie et dans l'Agriculture (F.R.I.A.), the Région Wallonne, the Université catholique de Louvain (UCLouvain), and the "Prix Pierre et Colette Bauchau" for financial support. J.W. thanks the Erasmus programme. This work was supported by the Agence National de la Recherche (ANR-12-BSV8-0008-04 and ANR-16-CE11-0006-01), Labex ARCANE (ANR-11-LABX-0003-01), and the Région Auvergne-Rhône-Alpes. The NanoBio-ICMG platforms (FR 2607) are acknowledged for their support. We also thank Dr. L. Troian-Gautier for scientific advice concerning the synthesis of CPITAP, Dr. L. Bonnat and Dr. T. Lavergne for providing biomolecular systems **A–D**, and Prof. F. Loiseau for help with the measurement of luminescence lifetimes. M.-C. Eloy is thanked for help with the confocal microscopy experiments. We thank L. Vriamont for the cover artwork.

Conflict of interest

The authors declare no conflict of interest.

Keywords: DNA structures · G-quadruplexes · photocytotoxicity · photo-electron transfer · ruthenium complexes

[1] D. R. Boer, A. Canals, M. Coll, *Dalton Trans.* **2009**, 399 – 414.
[2] H. J. Lipps, D. Rhodes, *Trends Cell Biol.* **2009**, *19*, 414 – 422.
[3] M. L. Bochman, K. Paeschke, V. A. Zakian, *Nat. Rev. Genet.* **2012**, *13*, 770 – 780.
[4] T. Simonsson, *Biol. Chem.* **2001**, *382*, 621 – 628.
[5] A. Siddiqui-Jain, C. L. Grand, D. J. Bearss, L. H. Hurley, *Proc. Natl. Acad. Sci. USA* **2002**, *99*, 11593 – 11598.
[6] M. Métifiot, S. Amrane, S. Litvak, M.-L. Andreola, *Nucleic Acids Res.* **2014**, *42*, 12352 – 12366.
[7] G. Biffi, M. Di Antonio, D. Tannahill, S. Balasubramanian, *Nat. Chem.* **2014**, *6*, 75 – 80.
[8] G. Biffi, D. Tannahill, J. McCafferty, S. Balasubramanian, *Nat. Chem.* **2013**, *5*, 182 – 186.
[9] A. Laguerre, K. Hukezalie, P. Winckler, F. Katranji, G. Chanteloup, M. Pirrotta, J.-M. Perrier-Cornet, J. M. Y. Wong, D. Monchaud, *J. Am. Chem. Soc.* **2015**, *137*, 8521 – 8525.
[10] A. De Cian, L. Lacroix, C. Douarre, N. Temime-Smaali, C. Trentesaux, J.-F. Riou, J.-L. Mergny, *Biochimie* **2008**, *90*, 131 – 155.
[11] D. J. Patel, A. T. Phan, V. Kuryavyi, *Nucleic Acids Res.* **2007**, *35*, 7429 – 7455.
[12] D. Hanahan, R. A. Weinberg, *Cell* **2011**, *144*, 646 – 674.
[13] T. M. Bryan, A. Englezou, L. Dalla-Pozza, M. A. Dunham, R. R. Reddel, *Nat. Med.* **1997**, *3*, 1271 – 1274.
[14] A. J. Cesare, R. R. Reddel, *Nat. Rev. Genet.* **2010**, *11*, 319 – 330.
[15] H. Han, L. H. Hurley, *Trends Pharmacol. Sci.* **2000**, *21*, 136 – 142.
[16] D. Monchaud, M.-P. Teulade-Fichou, *Org. Biomol. Chem.* **2008**, *6*, 627 – 636.
[17] P. Murat, Y. Singh, E. Defrancq, *Chem. Soc. Rev.* **2011**, *40*, 5293 – 5307.
[18] D. Yang, K. Okamoto, *Future Med. Chem.* **2010**, *2*, 619 – 646.
[19] B. R. Vummidi, J. Alzeer, N. W. Luedtke, *ChemBioChem* **2013**, *14*, 540 – 558.
[20] S. Neidle, *Nat. Rev. Chem.* **2017**, *1*, 0041.
[21] M. Nadai, F. Doria, L. Germani, S. N. Richter, M. Freccero, *Chem. Eur. J.* **2015**, *21*, 2330 – 2334.
[22] S. N. Georgiades, N. H. Abdkarim, K. Suntharalingam, R. Vilar, *Angew. Chem. Int. Ed.* **2010**, *49*, 4020 – 4034; *Angew. Chem.* **2010**, *122*, 4114 – 4128.
[23] Q. Cao, Y. Li, E. Freisinger, P. Z. Qin, R. K. O. Sigel, Z.-W. Mao, *Inorg. Chem. Front.* **2017**, *4*, 10 – 32.
[24] R. Kieltyka, P. Englebienne, J. Fakhoury, C. Autexier, N. Moitessier, H. F. Sleiman, *J. Am. Chem. Soc.* **2008**, *130*, 10040 – 10041.
[25] K. J. Castor, Z. Liu, J. Fakhoury, M. A. Hancock, A. Mittermaier, N. Moitessier, H. F. Sleiman, *Chem. Eur. J.* **2013**, *19*, 17836 – 17845.
[26] D. L. Ang, B. W. J. Harper, L. Cubo, O. Mendoza, R. Vilar, J. Aldrich-Wright, *Chem. Eur. J.* **2016**, *22*, 2317 – 2325.
[27] S. Ghosh, O. Mendoza, L. Cubo, F. Rosu, V. Gabelica, A. J. P. White, R. Vilar, *Chem. Eur. J.* **2014**, *20*, 4772 – 4779.
[28] M. Trajkovski, E. Morel, F. Hamon, S. Bombard, M.-P. Teulade-Fichou, J. Plavec, *Chem. Eur. J.* **2015**, *21*, 7798 – 7807.
[29] N. H. Campbell, N. H. A. Karim, G. N. Parkinson, M. Gunaratnam, V. Petrucci, A. K. Todd, R. Vilar, S. Neidle, *J. Med. Chem.* **2012**, *55*, 209 – 222.
[30] C. Q. Zhou, T. C. Liao, Z. Q. Li, J. Gonzalez-Garcia, M. Reynolds, M. Zou, R. Vilar, *Chem. Eur. J.* **2017**, *23*, 4713 – 4722.
[31] A. Ali, M. Kamra, S. Roy, K. Muniyappa, S. Bhattacharya, *Bioconjugate Chem.* **2017**, *28*, 341 – 352.
[32] X. Chen, J. H. Wu, Y. W. Lai, R. Zhao, H. Chao, L. N. Ji, *Dalton Trans.* **2013**, *42*, 4386 – 4397.
[33] L. Xu, X. Chen, J. Wu, J. Wang, L. Ji, H. Chao, *Chem. Eur. J.* **2015**, *21*, 4008 – 4020.
[34] X. Wang, L. Pei, X. Fan, S. Shi, *Inorg. Chem. Commun.* **2016**, *72*, 7 – 12.
[35] S. Lin, L. Lu, T.-S. Kang, J.-L. Mergny, C.-H. Leung, D.-L. Ma, *Anal. Chem.* **2016**, *88*, 10290 – 10295.
[36] K. J. Castor, K. L. Metera, U. M. Tefashe, C. J. Serpell, J. Mauzeroll, H. F. Sleiman, *Inorg. Chem.* **2015**, *54*, 6958 – 6967.
[37] L. Lu, M. Wang, Z. Mao, T.-S. Kang, X.-P. Chen, J.-J. Lu, C.-H. Leung, D.-L. Ma, *Sci. Rep.* **2016**, *6*, 22458.
[38] F. E. Poynton, S. A. Bright, S. Blasco, D. C. Williams, J. M. Kelly, T. Gunnlaugsson, *Chem. Soc. Rev.* **2017**, *46*, 7706 – 7756.
[39] Q. Deraedt, L. Marcelis, F. Loiseau, B. Elias, *Inorg. Chem. Front.* **2017**, *4*, 91 – 103.
[40] A. N. Boynton, L. Marcélis, A. J. McConnell, J. K. Barton, *Inorg. Chem.* **2017**, *56*, 8381 – 8389.
[41] G. Piraux, L. Bar, M. Abraham, T. Lavergne, H. Jamet, J. Dejeu, L. Marcélis, E. Defrancq, B. Elias, *Chem. Eur. J.* **2017**, *23*, 11872 – 11880.
[42] A. Masschelein, L. Jacquet, A. Kirsch-De Mesmaeker, J. Nasielski, *Inorg. Chem.* **1990**, *29*, 855 – 860.
[43] L. Marcélis, J. Ghesquière, K. Garnir, A. Kirsch-De Mesmaeker, C. Moucheron, *Coord. Chem. Rev.* **2012**, *256*, 1569 – 1582.
[44] C. S. Burke, A. Byrne, T. E. Keyes, *J. Am. Chem. Soc.* **2018**, *140*, 6945 – 6955.
[45] S. M. Cloonan, R. B. P. Elmes, M. Erby, S. A. Bright, F. E. Poynton, D. E. Nolan, S. J. Quinn, T. Gunnlaugsson, D. C. Williams, *J. Med. Chem.* **2015**, *58*, 4494 – 4505.

[46] S. Rickling, L. Ghisdavu, F. Pierard, P. Gerbaux, M. Surin, P. Murat, E. Defrancq, C. Moucheron, A. Kirsch-De Mesmaeker, *Chem. Eur. J.* **2010**, *16*, 3951 – 3961.
[47] F. Heinemann, J. Karges, G. Gasser, *Acc. Chem. Res.* **2017**, *50*, 2727 – 2736.
[48] K. J. Castor, J. Mancini, J. Fakhoury, N. Weill, R. Kieltyka, P. Englebienne, N. Avakyan, A. Mittermaier, C. Autexier, N. Moitessier, H. F. Sleiman, *ChemMedChem* **2012**, *7*, 85 – 94.
[49] L. Herman, S. Ghosh, E. Defrancq, A. Kirsch-De Mesmaeker, *J. Phys. Org. Chem.* **2008**, *21*, 670 – 681.
[50] I. Ortmans, B. Elias, J. M. Kelly, C. Moucheron, A. Kirsch-De Mesmaeker, *Dalton Trans.* **2004**, 668 – 676.
[51] A. M. Brouwer, *Pure Appl. Chem.* **2011**, *83*, 2213 – 2228.
[52] B. Elias, A. Kirsch-De Mesmaeker, *Coord. Chem. Rev.* **2006**, *250*, 1627 – 1641.
[53] S. P. Foxon, M. A. H. Alamiry, M. G. Walker, A. J. H. M. Meijer, I. V. Sazanovich, J. A. Weinstein, J. A. Thomas, *J. Phys. Chem. A* **2009**, *113*, 12754 – 12762.
[54] A. Boisdenghien, C. Moucheron, A. Kirsch-De Mesmaeker, *Inorg. Chem.* **2005**, *44*, 7678 – 7685.
[55] S. Steenken, S. V. Jovanovic, *J. Am. Chem. Soc.* **1997**, *119*, 617 – 618.
[56] J. Wallner, G. Lhota, D. Jeschek, A. Mader, K. Vorauer-Uhl, *J. Pharm. Biomed. Anal.* **2013**, *72*, 150 – 154.
[57] P. Murat, R. Bonnet, A. Van der Heyden, N. Spinelli, P. Labbé, D. Monchaud, M.-P. Teulade-Fichou, P. Dumy, E. Defrancq, *Chem. Eur. J.* **2010**, *16*, 6106 – 6114.
[58] R. Bonnet, T. Lavergne, B. Gennaro, N. Spinelli, E. Defrancq, *Chem. Commun.* **2015**, *51*, 4850 – 4853.
[59] P. Murat, D. Cressend, N. Spinelli, A. Van der Heyden, P. Labbé, P. Dumy, E. Defrancq, *ChemBioChem* **2008**, *9*, 2588 – 2591.
[60] L. Bonnat, L. Bar, B. Génnaro, H. Bonnet, O. Jarjayes, F. Thomas, J. Dejeu, E. Defrancq, T. Lavergne, *Chem. Eur. J.* **2017**, *23*, 5602 – 5613.
[61] L. Bonnat, J. Dejeu, H. Bonnet, B. Génnaro, O. Jarjayes, F. Thomas, T. Lavergne, E. Defrancq, *Chem. Eur. J.* **2016**, *22*, 3139 – 3147.
[62] C. M. Incles, C. M. Schultes, H. Kempski, H. Koehler, L. R. Kelland, S. Neidle, *Mol. Cancer Ther.* **2004**, *3*, 1201 – 1206.
[63] The other complexes could not be used because of their lower quantum yield of emission (complex **2**) or their photoreactivity (complexes **3** and **4** undergo PET with guanine residues, which quenches the excited state). Their luminescence in the cells is thus too weak to be detected by confocal microscopy.
[64] L. Jacquet, A. Kirsch-De Mesmaeker, *J. Chem. Soc. Faraday Trans.* **1992**, *88*, 2471 – 2480.
[65] C. Hiort, P. Lincoln, B. Norden, *J. Am. Chem. Soc.* **1993**, *115*, 3448 – 3454; C. Moucheron, A. Kirsch-De Mesmaeker, S. Choua, *Inorg. Chem.* **1997**, *36*, 584 – 592.

Manuscript received: September 18, 2018
Revised manuscript received: October 22, 2018
Accepted manuscript online: October 26, 2018
Version of record online: December 11, 2018